INTERNATIONAL JOURNAL FOR NUMERICAL AND ANALYTICAL METHODS IN GEOMECHANICS
Int. J. Numer. Anal. Meth. Geomech., **22**, 903–919 (1998)

BIFURCATIONS OF THICK-WALLED HOLLOW CYLINDERS OF GEOMATERIALS UNDER AXISYMMETRIC COMPRESSION

K. T. CHAU[1,*] AND S. K. CHOI[2]

[1] *Department of Civil and Structural Engineering, The Hong Kong Polytechnic University, Hung Hom, Kowloon, Hong Kong, SAR, China*
[2] *Division of Petroleum Resources, CSIRO, Kinnoull Grove, Syndal Victoria 3150, Australia*

SUMMARY

This paper derives analytically the condition for the onset of diffuse mode bifurcations in thick-walled hollow cylinders with internal radius a, external radius b and length L under axial compression and confining pressure. The thick-walled cylindrical specimens are made of geomaterial characterized by Rudnicki's constitutive model,[36] and the method of solution for the governing equations is the velocity potential approach employed by Chau.[37, 38] Numerical results show that thick-walled cylinders are stronger than thin-walled cylinders against diffuse mode bifurcations, including both buckling, axisymmetric and non-axisymmetric deformations. In contrast to the conclusion for solid cylinders (Chau[37,38]), no buckling solution is found for $\gamma = m\pi a/L$ smaller than about 0·7 under compression for a fixed and finite value of a/b (i.e. no buckling for long and slender hollow cylinders with small a/L and fixed b/a). When $0{\cdot}7 < \gamma < 0{\cdot}9$, buckling is the expected first bifurcation; whereas, when $\gamma > 0{\cdot}9$, bulging or barrelling is anticipated. The exact value of γ that excludes buckling and separates the buckling and barrelling phenomena depends on the current values of the constitutive parameters of the solid. Hollow cylinders with higher degree of anisotropy, disobeying normality flow rule, and subjected to confining pressure are more conducive to bifurcations than cylinders made of materials with isotropy, obeying normality, and subjected to no confining pressure. In addition, diffuse mode bifurcations are found possible in the pre-peak regime of the stress–strain curve.

Key words: hollow cylinders; diffuse mode bifurcations; geomaterials; non-normality; pressure-sensitivity

1. INTRODUCTION

In recent years, both thick-walled and thin-walled hollow cylinders have been found extremely useful in the testing of both soils and rocks, although the first use of hollow cylinder test in rock mechanics is probably by Adam[1] and in soil mechanics by Kirkpatrick.[2] One of the main advantages of hollow cylinder test is its capability in applying torsion, confining stress and axial compression simultaneously.[3] For example, it has been used in estimating the change of the tangential shear modulus with axial deformation, which was done by applying a small torque to

*Correspondence to: K. T. Chau, Department of Civil and Structural Engineering, The Hong Kong Polytechnic University, Hung Hom, Kowloon, Hong Kong, SAR, China, E-mail: cektchau@polyu.edu.hk.

Contract grant sponsor: The Hong Kong Polytechnic University; contract grant sponsor: CSIRO; contract grant sponsor: RGC; contract grant number: Earmarked grant No. 0357-052; contract grant number: Earmarked grant No.: 0357-025

CCC 0363–9061/98/110903–17$17.50 *Received 5 May 1997*
Revised 17 December 1997

the hollow cylinders at various stages of triaxial tests;[4] and the results are extremely useful in predicting the onset of localization since previous bifurcation analyses have demonstrated that the predictions are sensitive to the values of moduli governing abrupt changes in the pattern of deformation (e.g. References 5 and 6).

In studying borehole instabilities and failure mechanisms of tunnels, numerous experiments on thick-walled hollow cylinders of rocks have been done (e.g. References 1, 7–14). Types of rocks or rock-like materials that have been tested include limestone,[15] artificial material,[16, 17] dolomite,[18] sandstone,[19] marble[4] and 'Johnstone' of Choi,[20] and Johnston and Choi[21] (Cox[22] private communication). Thick-walled hollow cylinder tests have also been used in soil mechanics to calibrate the yield function in sand and clay (e.g. References 2 and 23), to simulate the pressuremeter test in laboratory,[24] and to investigate the onset of bifurcations[25, 26] and in the study of the recrystallization of ice under stress.[27] In short, experiments on thick-walled hollow cylinders have been found useful in providing information on the failure mechanisms, on the conditions for strain localization, and on the patterns of geometric bifurcations of deformation or breakout near boreholes or tunnels.

A stress analysis for thick-walled cylinders was done by Biot[28] using the holograph method. When the effect of damage is incorporated, a nonlinear stress analysis is proposed by Pellegrino *et al.*[29] Related to the hollow cylinder tests, bifurcation analyses for borehole instabilities have been proposed.[30–34] Due to mathematical difficulties, the bifurcation problem of thick-walled cylinders has been solved by either assuming the bifurcation as a surface instability or by using finite element analysis.[31, 32] For the buckling analysis of thick orthotropic and transversely isotropic cylindrical shells, Kardomateas[34, 35] considered a series of bifurcation analyses, which are based upon three dimensional theory of elasticity, and thus similar to the one to be presented in this paper. However, Kardomateas' analyses are motivated for the shell buckling in composite structures; therefore, the essential characteristics of geomaterials, including pressure-sensitivity and dilatancy, are not included in his analyses. To the best of our knowledge, no analytic solution for the onset condition of bifurcation exists for thick-walled cylinders of geomaterials under axial compression and confining pressure.

The main purpose of this paper is to provide an analytic solution for the simplest bifurcation problem of the thick-walled hollow cylinder test for geomaterials under axial compression with equal internal and external pressures. The ends of the cylinders are loaded by a prescribed velocity with no shear traction; and a constant lateral pressure is applied on the inner and outer surfaces of the hollow cylinders with zero traction rate. Uniform deformation of the cylinder is considered as the trivial solution to the governing equations for the cylinder when it is subjected to disturbance, and we investigate the condition under which the uniform state gives way to a non-uniform deformation field (i.e. bifurcation occurs). The incremental linear constitutive model by Rudnicki,[36] which incorporates the features of most geomaterials like pressure-sensitivity, dilatancy, and transverse anisotropy and has also been used by Chau,[37–39] is used here to characterize our thick-walled cylinders under axial compression with equal internal and external confining pressure. The approach of velocity potentials, which is modified from the displacement potentials by Hu[40] for elastic analysis and is proposed by Chau,[38, 41] is adopted in the present analysis. The main idea of this approach is to uncouple the three equations of continued equilibrium for the bifurcation problem by introducing two velocity potentials.

The condition for strain localization or shear band formation, which corresponds to the loss of ellipticity of the governing equations, is the same as those given by Chau,[38] and therefore, will not be discussed in detail here. Our main emphasis is on the geometric bifurcations induced by the

traction rate free surfaces (i.e. the cylindrical curved surfaces). Since non-axisymmetric mode of failure is always observed in experiments (e.g. Reference 19), symmetric, antisymmetric and all higher circumferential modes of bifurcation will be considered in the present analysis.

One main limitation of the present analysis is that the internal and external pressures have been assumed to be equal; whereas in usual experiments the internal pressure is normally reduced, after both internal and external pressures are raised to a suitable level, until bifurcation or failure occurs so as to simulate the process of borehole excavation. Nevertheless, the present bifurcation analysis should provide a pilot study for the later more complicated bifurcation analysis.

In addition, for real experiments on thick-walled cylinders the process of progressive failure, which may precede or follow the onset of material or geometric bifurcation, is very important in understanding the process of failure. In this connection, we should mention the numerical simulation by Papanastasiou and Vardoulakis[33] on hollow cylinders of Cosserat continuum with a modified Mohr–Coulomb flow theory of plasticity. To capture the process of spalling and breakout (e.g. van en Hoek *et al.*[42]), fracture mechanics together with buckling may be used (e.g. References 43–45). However, all these processes of progressive failure are out of the scope of the present study.

2. RUDNICKI'S (1977) CONSTITUTIVE MODEL

We consider a thick-walled hollow circular cylinder of internal radius a, external radius b, and length L under initial axisymmetric uniform deformations (see Figure 1). The current configuration is adopted as reference and the subsequent deformation of the material is characterized by the following incremental linear, time- and rate-independent constitutive model:[36]

$$\begin{aligned} \overset{\nabla}{\sigma}_{zz} &= \left(\frac{E + 9Kr^*v}{2}\right)D_{zz} + \frac{9Kr^*}{4}(D_{rr} + D_{\theta\theta}), \qquad \overset{\nabla}{\sigma}_{z\alpha} = 2G_l D_{z\alpha} \\ \overset{\nabla}{\sigma}_{\alpha\beta} &= 2G_t[D_{\alpha\beta} - \tfrac{1}{2}\,\delta_{\alpha\beta}(D_{rr} + D_{\theta\theta})] + \delta_{\alpha\beta}\frac{9K}{2}[vD_{zz} + \tfrac{1}{2}(D_{rr} + D_{\theta\theta})] \end{aligned} \tag{1}$$

with $\alpha, \beta = r, \theta$; and where (r, θ, z) are the cylindrical polar co-ordinates, $\boldsymbol{\sigma}$ is the Cauchy stress tensor, the superposed ∇ denotes the Jaumann or co-rotational rate,[46] and $\mathbf{D}$ is the rate of deformation tensor. As discussed by Rudnicki[36] and by Chau,[37, 38] E is the instantaneous tangent modulus, which is a very useful parameter indicating whether the stress state is pre- or post-peak because E decreases with deformation in the pre-peak regime, equals zero at the peak applied stress, and becomes negative in the post-peak regime. The axial straining is inhibited by the lateral stress rate by a factor of r^*, which can be interpreted as a pressure-sensitive parameter.[36, 37] The effective Poisson's ratio v is the tangent of the curve of lateral strain versus axial strain at constant confining stress (see Figure 2 of Reference 36). The incremental transverse and longitudinal shear moduli, and the in-plane bulk modulus are given by G_t, G_l, and K respectively. For detailed discussion of Rudnicki's model,[36] we refer to References 36 and 37. It is, however, helpful for later discussion to mention that $2v = r^*$ for the normality limit (i.e. the normals to the plastic potential and yield function are parallel). A simple way to calibrate r^* and v of Rudnicki's model[36] is to compare them with the limiting case of Rudnicki–Rice model[5] (e.g. see (3) of Chau[37]). Note that all these constitutive parameters are incremental values that change with the deformation.

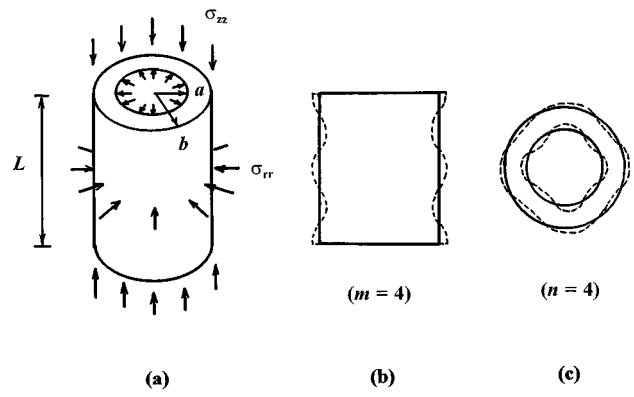

Figure 1. Thick-walled hollow cylinder test: (a) a sketch for the undeformed thick-walled hollow circular cylinder subjected to axial compression σ_{zz} and confining pressure σ_{rr}; (b) a side view of possible deformed shape of the hollow cylinders ($m = 4$); (c) a plan view of the possible deformed shape of the hollow cylinders ($n = 4$)

For general modes of deformations, the rate of deformation tensor **D** can be related to the velocity **v** in the polar coordinate (r, θ, z) as shown in (2.2) of Reference 38, and they will not be repeated here. For the expressions relating the physical components of the nominal stress rate $\dot{\mathbf{t}}$ to those of the Cauchy stress rates $\dot{\boldsymbol{\sigma}}$, the Cauchy stress $\boldsymbol{\sigma}$ and the velocity field **v**, we also refer to (2.3) of Reference 38.

3. GOVERNING EQUATIONS

We choose a cylindrical polar co-ordinate system (r, θ, z) with the origin resting on the bottom of the cylinder ($z = 0$) and the z-axis coinciding with the axis of symmetry. Presuming that the hollow circular cylinder deforms homogeneously up to the current state and a further homogeneous deformation is always a possible solution for the next increment of deformation, then an alternative solution for the next increment of deformation is sought by applying a perturbation field. The end boundary conditions should be satisfied by the difference in these incremental solutions (the homogeneous one and the bifurcation), which is denoted by the superscript *, as

$$v_z^* = 0, \qquad \dot{t}_{zr}^* = 0, \qquad \dot{t}_{z\theta}^* = 0 \quad \text{on } z = 0, L \tag{2}$$

which corresponds to a prescribed velocity in the z-direction at the end of the cylinder with no shear traction. When a constant lateral stress is applied in the r-direction with zero shear traction rate, the boundary conditions on the curved surfaces are

$$\dot{t}_{rr}^* = 0, \qquad \dot{t}_{rz}^* = 0, \qquad \dot{t}_{r\theta}^* = 0 \quad \text{on } r = a, b \tag{3}$$

As shown by Chau,[38] the continued equilibrium of both incremental solutions, $\nabla \cdot \dot{\mathbf{t}}^* = 0$, for the Rudnicki model[36] can be written in terms of **v** as

$$\left(G_t + \frac{9K}{4}\right)\frac{\partial e}{\partial r} + 2G_t \frac{1}{r}\frac{\partial \Omega_{r\theta}}{\partial \theta} + G_l(1+s)\frac{\partial^2 v_r}{\partial z^2} + \left[G_l(1-s) + \frac{9Kv}{2} - \left(G_t + \frac{9K}{4}\right)\right]\frac{\partial^2 v_z}{\partial r \partial z} = 0 \tag{4}$$

$$\left(G_t+\frac{9K}{4}\right)\frac{1}{r}\frac{\partial e}{\partial\theta}+2G_t\frac{\partial\Omega_{\theta r}}{\partial\theta}+G_l(1+s)\frac{\partial^2 v_\theta}{\partial z^2}+\left[G_l(1-s)+\frac{9Kv}{2}-\left(G_t+\frac{9K}{4}\right)\right]\frac{1}{r}\frac{\partial^2 v_z}{\partial\theta\partial z}=0 \tag{5}$$

$$\left(\frac{9Kr^*}{4}+2G_l\right)\frac{\partial e}{\partial z}+\left[E-2G_l-\frac{9Kr^*}{4}(1-2v)\right]\frac{\partial^2 v_z}{\partial z^2}+2G_l(1-s)\left[\frac{1}{r}\frac{\partial\Omega_{z\theta}}{\partial\theta}+\frac{1}{r}\frac{\partial}{\partial r}(r\Omega_{zr})\right]=0 \tag{6}$$

where

$$s=(\sigma_{zz}-\sigma_{rr})/2G_l,\qquad e=\frac{1}{r}\frac{\partial(rv_r)}{\partial r}+\frac{1}{r}\frac{\partial v_\theta}{\partial\theta}+\frac{\partial v_z}{\partial z} \tag{7}$$

and $\Omega=(\mathbf{L}-\mathbf{L}^{\mathrm{T}})/2$ is the anti-symmetric part of the velocity gradient tensor. Note that for the sake of simplicity all the asterisk *'s have been dropped in the above expressions, with the understanding that the velocity field $\mathbf{v}$ is the difference between the homogeneous solution and the bifurcation. The radial stress σ_{rr} is the applied confining stress on the cylindrical surfaces and the axial stress σ_{zz} is the unknown eigenstress at bifurcation when a prescribed velocity is imposed. In obtaining (4)–(6) we have assumed an initial axisymmetric stress state ($\sigma_{rr}=\sigma_{\theta\theta}$). This assumption actually restricts the applicability of (4)–(6) to the case of equal internal and external pressures, since unbalanced confining pressures on the inner and outer cylindrical surfaces of the hollow cylinder inevitably induce unequal σ_{rr} and $\sigma_{\theta\theta}$.

4. METHOD OF VELOCITY POTENTIALS

As mentioned in the Introduction, the velocity potential proposed by Chau,[38] which is modified from Hu's[40] displacement potentials for elastic problems, is adopted here. To uncouple equations (4)–(6), the following velocity potentials (Φ and Ψ) are introduced:[38]

$$v_r=\frac{\partial^2\Phi}{\partial r\partial z}+\frac{1}{r}\frac{\partial\Psi}{\partial\theta},\qquad v_\theta=\frac{1}{r}\frac{\partial^2\Phi}{\partial\theta\partial z}-\frac{\partial\Psi}{\partial r} \tag{8}$$

$$v_r=-\left[\frac{9K/4+G_t}{9Kv/2+G_l(1-s)}\right]\nabla_1\Phi-\left[\frac{G_l(1-s)}{9Kv/2+G_l(1-s)}\right]\frac{\partial^2\Phi}{\partial z^2} \tag{9}$$

where

$$\nabla_1=\frac{1}{r}\frac{\partial}{\partial r}\left(r\frac{\partial}{\partial r}\right)+\frac{1}{r^2}\frac{\partial^2}{\partial\theta^2} \tag{10}$$

Since the velocity components are defined in terms of these potentials, Φ and Ψ automatically satisfy compatibility condition. Substitution of (8)–(9) into (4)–(6), we find that the equations of continued equilibrium are satisfied exactly if Φ and Ψ satisfy

$$\left(\nabla_1-v_1^2\frac{\partial^2}{\partial z^2}\right)\left(\nabla_1-v_2^2\frac{\partial^2}{\partial z^2}\right)\Phi=0,\qquad \left(\nabla_1+v_3^2\frac{\partial^2}{\partial z^2}\right)\Psi=0 \tag{11}$$

where v_1 and v_2 satisfy

$$Av_\alpha^4+Bv_\alpha^2+C=0,\qquad(\alpha=1,2) \tag{12}$$

in which A, B, and C are defined as

$$A = (1 - s)(4G_t + 9K) \tag{13}$$

$$B = E(4G_t + 9K)/G_l + 9K[2r^*vG_t/G_l - (2v + r^*) + s(r^* - 2v)] \tag{14}$$

$$C = 2(1 + s)(9Kr^*v + 2E) \tag{15}$$

and v_3 is defined as

$$v_3 = [G_l(1 + s)/G_t]^{1/2} \tag{16}$$

Similar to the idea of introducing the Airy's stress function for two-dimensional elasticity, these velocity potentials Φ and Ψ have to satisfy both requirements of compatibility and continued equilibrium. Because of the fulfilment of these requirements, the stress rates and velocity field obtained for solving Φ and Ψ are the general solutions. In addition, the *coupled* differential equations in terms of $\mathbf{v}$ are now replaced by an *uncoupled* system of differential equations for Φ and Ψ. The price for reducing the unknowns to two and for uncoupling of the governing equations is that we now have to deal with fourth-order differential equation for Φ, instead of the second-order differential equations for $\mathbf{v}$.

With the introduction of the velocity potentials Φ and Ψ, the zero traction rate boundary conditions (3) can be rewritten, as shown in appendix. In addition, the Cauchy stress rates can also be expressed in terms of Φ and Ψ, which can be found in (5.5)–(5.10) of Chau[38] and will not be given here. As shown by Chau,[38] there exists a close resemblance between (12) and the characteristic equation for shear band, which can simply be obtained by identifying v_α as g/g_z, where $\mathbf{g}$ is the normal to the shear band and $g^2 = g_\theta^2 + g_r^2$. The first of (11) is elliptic, parabolic or hyperbolic if there are zero, two or four real roots for (12) respectively. As discussed by Chau,[38, 41] only the geometric bifurcations in the elliptic regime are meaningful as shear banding will be the dominant mode of failure in both the parabolic and hyperbolic regimes. If v_1 and v_2 are real or v_3 is imaginary, shear band mode occurs prior to the solutions obtained by solving (11) with the boundary conditions (2) and (3).

5. DIFFUSE BIFURCATION MODES

To satisfy the end boundary conditions on $z = 0, L$ given in (2), the following diffuse bifurcation modes can be assumed:[38]

$$\Phi = C_1\varphi(r)\sin(\eta z)\cos(n\theta), \qquad \Psi = C_2\psi(r)\cos(\eta z)\sin(n\theta) \tag{17}$$

where $\eta = m\pi/L$, with $m = 1, 2, \ldots$, and $n = 0, 1, \ldots,$; and C_1 and C_2 are arbitrary constants. A sketch for the deformation mode shapes predicted by (17) is illustrated in Figure 1. Substitution of (17) into (11) gives

$$(\nabla_2 + \eta^2 v_1^2)(\nabla_2 + \eta^2 v_2^2)\varphi = 0, \qquad (\nabla_2 - \eta^2 v_3^2)\psi = 0 \tag{18}$$

where

$$\nabla_2 = \frac{1}{r}\frac{\mathrm{d}}{\mathrm{d}r}\left(r\frac{\mathrm{d}}{\mathrm{d}r}\right) - \frac{n^2}{r^2} \tag{19}$$

Guided by the observation of Chau,[38] the first geometric bifurcation is likely to be encountered before shear band becoming possible and should be in the elliptic complex (EC) regime, that is, the roots for v_α are complex conjugates. Therefore, only geometric bifurcation in the EC regime will be considered here. In particular, the general solution for φ is

$$\varphi = A_1 J_n(\eta v r) + \bar{A}_1 J_n(\eta \bar{v} r) + A_2 Y_n(\eta v r) + \bar{A}_2 Y_n(\eta \bar{v} r) \tag{20}$$

where J_n and Y_n are the Bessel functions of the first and second kinds, and A_1 and A_2 are complex constants. The superposed bar implies the complex conjugate. And the complex conjugate pairs of v_α are $v = p + \mathrm{i}q$ and $\bar{v} = p - \mathrm{i}q$ [where $\mathrm{i} = (-1)^{1/2}$ is the imaginary constant]; and, p and q are defined as

$$p^2 - q^2 = -B/2A, \qquad p^2 + q^2 = (C/A)^{1/2} \tag{21}$$

where A, B and C are given in (13)–(15). For v_3^2 greater than zero, the general solution for Ψ is

$$\Psi = D_1 I_n(\eta v_3 r) + D_2 K_n(\eta v_3 r) \tag{22}$$

where I_n and K_n are the modified Bessel functions of the first and second kinds, D_1 and D_2 are real constants, and v_3 is given in (16). Substitution of the diffuse modes of (20) and (22) into the curved boundary conditions (38)–(40) on $r = a, b$ given in the appendix leads to a homogeneous system of six equations for the unknowns constants $\mathrm{Re}(A_1)$, $\mathrm{Im}(A_1)$, $\mathrm{Re}(A_2)$, $\mathrm{Im}(A_2)$, D_1 and D_2, where $\mathrm{Im}(\dots)$ and $\mathrm{Re}(\dots)$ stand for the imaginary and real parts of $(\dots)$. For non-trivial solutions for the bifurcation field to exist, we must set the determinant of the system of equations to zero. That is, we have

$$\begin{vmatrix}
2\eta^3 X_R(\gamma) & -2\eta^3 X_I(\gamma) & W_1(\gamma) & 2\eta^3 X_R^*(\gamma) & -2\eta^3 X_I^*(\gamma) & W_1^*(\gamma) \\
2\eta^3 X_R(\alpha\gamma) & -2\eta^3 X_I(\alpha\gamma) & W_1(\alpha\gamma) & 2\eta^3 X_R^*(\alpha\gamma) & -2\eta^3 X_I^*(\alpha\gamma) & W_1^*(\alpha\gamma) \\
2\eta Y_R(\gamma) & -2\eta Y_I(\gamma) & W_2(\gamma) & 2\eta Y_R^*(\gamma) & -2\eta Y_I^*(\gamma) & W_2^*(\gamma) \\
2\eta Y_R(\alpha\gamma) & -2\eta Y_I(\alpha\gamma) & W_2(\alpha\gamma) & 2\eta X_R^*(\alpha\gamma) & -2\eta Y_I^*(\alpha\gamma) & W_2^*(\alpha\gamma) \\
2\eta Z_R(\gamma) & -2\eta Z_I(\gamma) & W_3(\gamma) & 2\eta Z_R^*(\gamma) & -2\eta Z_I^*(\gamma) & W_3^*(\gamma) \\
2\eta Z_R(\alpha\gamma) & -2\eta Z_I(\alpha\gamma) & W_3(\alpha\gamma) & 2\eta Z_R^*(\alpha\gamma) & -2\eta Z_I^*(\alpha\gamma) & W_3^*(\alpha\gamma)
\end{vmatrix} = 0 \tag{23}$$

where $\gamma = \eta a$, $\alpha = b/a > 1$ and the subscripts I and R denote the imaginary and real parts of a complex function (e.g. X_I and X_R are the imaginary and real part of the complex function X). The complex functions $X(\gamma)$, $X^*(\gamma)$, $Y(\gamma)$, $Y^*(\gamma)$, $Z(\gamma)$, $Z^*(\gamma)$, which involve only Bessel functions of the first and second kinds, are defined as

$$X(\gamma) = 2[2Y_2 + v^2(2Y_1 + Y_3)]J_n(v\gamma) - v^2 Y_3[(J_{n-2}(v\gamma) + J_{n+2}(v\gamma)] \tag{24}$$

$$X^*(\gamma) = 2[2Y_2 + v^2(2Y_1 + Y_3)]Y_n(v\gamma) - v^2 Y_3[(Y_{n-2}(v\gamma) + Y_{n+2}(v\gamma)] \tag{25}$$

$$Y(\gamma) = v(v^2 Y_4 + Y_5)[J_{n-1}(v\gamma) - J_{n+1}(v\gamma)] \tag{26}$$

$$Y^*(\gamma) = v(v^2 Y_4 + Y_5)[Y_{n-1}(v\gamma) - Y_{n+1}(v\gamma)] \tag{27}$$

$$Z(\gamma) = 2nY_3 v^2\left[2\frac{J_n(v\gamma)}{(v\gamma)^2} + \frac{J_{n+1}(v\gamma) - J_{n-1}(v\gamma)}{v\gamma}\right] \tag{28}$$

$$Z^*(\gamma) = 2nY_3 v^2\left[2\frac{Y_n(v\gamma)}{(v\gamma)^2} + \frac{Y_{n+1}(v\gamma) - Y_{n-1}(v\gamma)}{v\gamma}\right] \tag{29}$$

where, again, $v = p + \mathrm{i}q$ with p and q defined in (21). In addition, Y_i $(i = 1, 2, \ldots, 8)$ are defined in (41)–(43) in the appendix and should not be confused with the Bessel function of the second kind $Y_n(v\gamma)$. And, the complex functions $W_1(\gamma)$, $W_1^*(\gamma)$, $W_2(\gamma)$, $W_2^*(\gamma)$, $W_3(\gamma)$ and $W_3^*(\gamma)$, which involve only the modified Bessel functions of the first and second kinds, are given by

$$W_1(\gamma) = -\frac{2nv_3^2 Y_3}{(v_3\gamma)^2}\{v_3\gamma[I_{n-1}(v_3\gamma) + I_{n+1}(v_3\gamma)] - 2I_n(v_3\gamma)\} \tag{30}$$

$$W_1^*(\gamma) = \frac{2nv_3^2 Y_3}{(v_3\gamma)^2}\{v_3\gamma[K_{n-1}(v_3\gamma) + K_{n+1}(v_3\gamma)] + 2K_n(v_3\gamma)\} \tag{31}$$

$$W_2(\gamma) = 2nv_3 Y_6 \frac{I_n(v_3\gamma)}{v_3\gamma}, \qquad W_2^*(\gamma) = 2nv_3 Y_6 \frac{K_n(v_3\gamma)}{v_3\gamma} \tag{32}$$

$$W_3(\gamma) = v_3^2\left\{\frac{2Y_7}{v_3\gamma}\left[I_{n-1}(v_3\gamma) + I_{n+1}(v_3\gamma) - 2n^2\frac{I_n(v_3\gamma)}{v_3\gamma}\right] - Y_8[I_{n-2}(v_3\gamma) + 2I_n(v_3\gamma) + I_{n+2}(v_3\gamma)]\right\} \tag{33}$$

$$W_3^*(\gamma) = -v_3^2\left\{\frac{2Y_7}{v_3\gamma}\left[K_{n-1}(v_3\gamma) + K_{n+1}(v_3\gamma) + 2n^2\frac{K_n(v_3\gamma)}{v_3\gamma}\right] + Y_8[K_{n-2}(v_3\gamma) + 2K_n(v_3\gamma) + K_{n+2}(v_3\gamma)]\right\} \tag{34}$$

The next section will discuss the numerical solution for $s = (\sigma_{zz} - \sigma_{rr})/(2G_l)$ which satisfies (23).

6. NUMERICAL RESULTS AND DISCUSSION

The numerical calculation of the eigenstress at bifurcation can be done using standard root search technique (e.g. Reference 47). The evaluation of the modified Bessel functions with real arguments can be found in standard textbooks (e.g. Reference 47), however, for the calculation of the Bessel function of the first and second kinds with complex arguments more specialized subroutines (e.g. References 48–53) have to be used. The results by the subroutine for Bessel functions of the first kind with complex argument have been checked with existing tables (e.g. Reference 54). However, numerical tables for the Bessel function of the second kind with complex argument cannot be found easily in the literature. One alternative is to check the numerical values of the Kelvin functions ($\mathrm{ker}_v x$ and $\mathrm{kei}_v x$), which can be expressed in terms of the Bessel functions of the first and second kinds with complex arguments as[55]

$$\mathrm{ker}_v x + \mathrm{i}\,\mathrm{kei}_v x = \tfrac{1}{2}\pi\mathrm{i}H_v^{(1)}(x\mathrm{e}^{3\pi\mathrm{i}/4}) = \tfrac{1}{2}\pi[\mathrm{i}J_v(x\mathrm{e}^{3\pi\mathrm{i}/4}) - Y_v(x\mathrm{e}^{3\pi\mathrm{i}/4})] \tag{35}$$

where $H_v^{(1)}$ is the Hankel function. Equating the real and imaginary parts of (35) yields:

$$\mathrm{ker}_v x = -\frac{\pi}{2}\{\mathrm{Im}[J_v(x\mathrm{e}^{3\pi\mathrm{i}/4})] + \mathrm{Re}[Y_v(x\mathrm{e}^{3\pi\mathrm{i}/4})]\} \tag{36}$$

$$\mathrm{kei}_v x = \frac{\pi}{2}\{\mathrm{Re}[J_v(x\mathrm{e}^{3\pi\mathrm{i}/4})] - \mathrm{Im}[Y_v(x\mathrm{e}^{3\pi\mathrm{i}/4})]\} \tag{37}$$

Therefore, Table 9.12 of Abramowitz and Stegun[55] can be used for checking purposes.

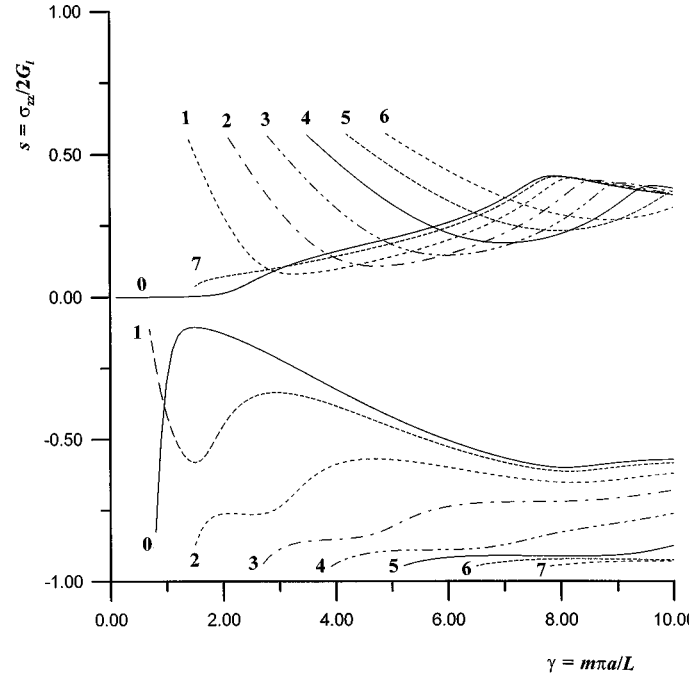

Figure 2. Normalized stress $s = \sigma_{zz}/(2G_l)$ versus $\gamma = m\pi a/L$ at the onset of bifurcation. The circumferential mode number n varies from 0 to 7. Other parameters for the plots are: $E/G_l = 0$, $G_t/G_l = 0{\cdot}75$, $\mu = \beta = 0{\cdot}4$, $G_l/K = 0{\cdot}2$, $b/a = 1{\cdot}5$ and $\sigma_{rr} = 0$

In the following analysis, we have assumed that v and r^* in Rudnicki's[36] model can be interpreted from the parameters of the Rudnicki–Rice[5] model; in particular, (3) of Chau[37] relates v and r^* in terms of the internal friction coefficient and the dilatancy factor (μ and β) of the Rudnicki–Rice[5] model. Note that whenever this identification is made, v and r^* change sign with $s = (\sigma_{zz} - \sigma_{rr})/(2G_l)$. As calibrated by Rudnicki and Rice,[5] the typical range for β is 0·2–0·4 and for μ is 0·4–0·9; these values yield $v \approx 0{\cdot}7$–$0{\cdot}95$ and $r^* \approx 1{\cdot}9$–$4{\cdot}25$ under compression. To capture the effect of the constitutive parameters on the condition of bifurcations in a reasonably simple way, the eigenvalue surfaces to be given below are evaluated by holding all parameters except one constant. In general, it may not be true in real situation as the material parameters in Rudnicki[36] model may evolve in a complex manner under external compressions.

Figure 2 plots the normalized stress $s = \sigma_{zz}/(2G_l)$ at the onset of bifurcation versus the geometric parameter $\gamma = m\pi a/L$ with various values of the circumferential mode number n ranging from 0 to 7. Although we have only calculated the bifurcation modes with n up to 7, calculations for higher bifurcation modes ($n > 7$) involve no additional difficulty. The hollow cylinder is assumed to obey the normality flow rule (i.e $\mu = \beta = 0{\cdot}4$) and the bifurcation is assumed to occur at the peak applied stress (i.e. $E = 0$). Whether this assumption is valid for a particular geomaterial depends on the evolution of E with the applied stress. The main purpose of Figure 2 is to illustrate the parameter-dependency of our eigenvalue equation. Other parameters used in these plot are $G_t/G_l = 0{\cdot}75$, $G_l/K = 0{\cdot}2$, $b/a = 1{\cdot}5$ and $\sigma_{rr} = 0$. All of these geometric bifurcations occur in the EC-regime and, hence, precede the formation of shear

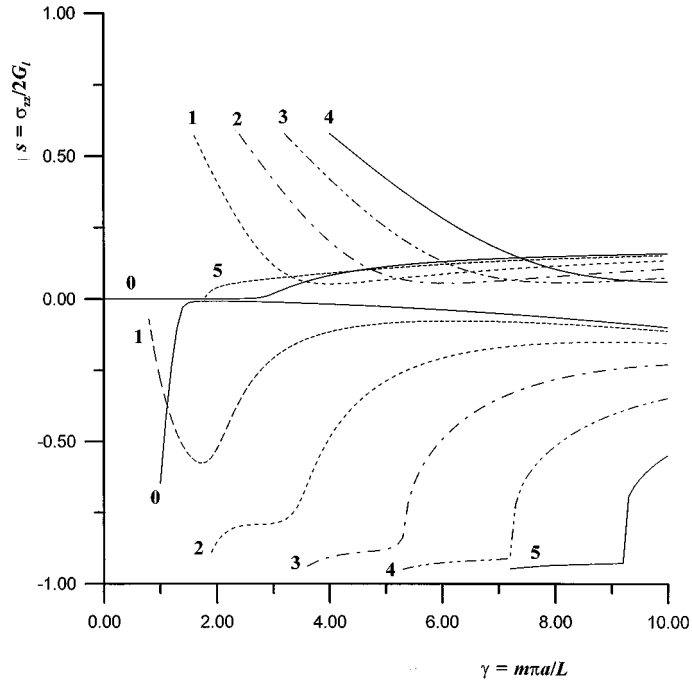

Figure 3. Normalized stress $s = \sigma_{zz}/(2G_t)$ versus $\gamma = m\pi a/L$ at the onset of bifurcation. The circumferential mode number n varies from 0 to 5. All parameters same as those used in Figure 2 except $b/a = 1{\cdot}1$

banding or the onset of strain localization. In contrast to the prediction for solid cylinders (e.g. References 38 and 41), no anti-symmetric solution ($n = 1$) is found for γ smaller than 0·7 under compression or with $s < 0$ (i.e Euler's buckling formula is no longer obtained as the special case) for a fixed and finite value of b/a. For $\gamma > 0{\cdot}9$, geometric bifurcation always appears in the form of barrelling or axisymmetric deformation (i.e $n = 0$); and buckling type of deformation ($n = 1$) only dominates when $0{\cdot}7 < \gamma < 0{\cdot}9$. Therefore, if these bifurcation solutions are going to trigger the onset of non-uniform deformation or progressive failure, any point on the inner surfaces ($r = a$) can be the center of nucleation of the non-uniform deformation. In real experiments, the point of nucleation of non-uniform deformation probably depends on the location of the defects in the geomaterial. Under extension tests ($s > 0$), a richer variety of bifurcation solutions with different values of n become available, depending on the exact values of the geometric ratio a/L. But, in general, a higher stress level is required for a higher circumferential mode (i.e. larger value of n) to becoming possible. The plots of the bifurcation stress given in Figure 2 will be used as a reference for comparison in the following discussions.

Figures 3 and 4 illustrates the effect of the thickness of the hollow cylinders on the bifurcation stresses by using b/a equal to 1·1 (thin-walled cylinders) and 3·0 (very small circular opening). All other parameters used in these figures are the same as those given in Figure 2. As expected, the bifurcation stress decreases drastically with the reduction of the thickness of the hollow cylinders, but increases monotonically with the thickness ratio b/a (or in other words the cylinders become stronger with b/a).

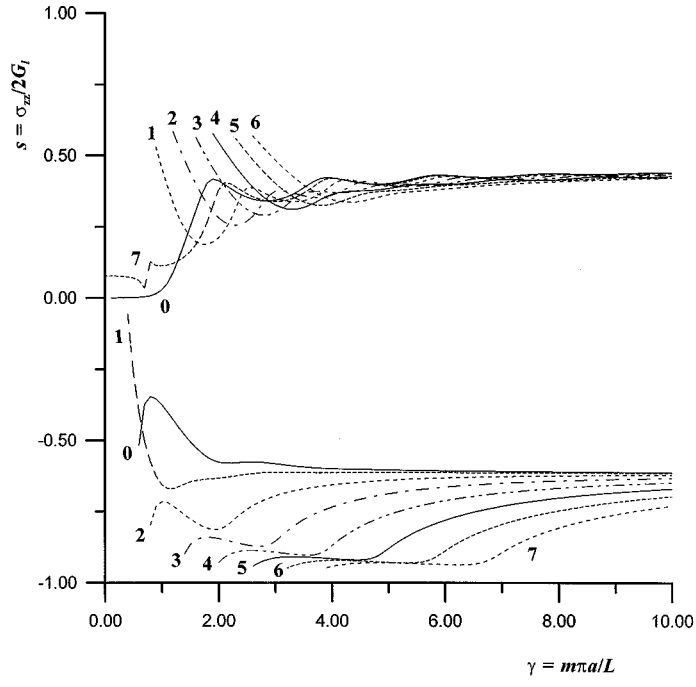

Figure 4. Normalized stress $s = \sigma_{zz}/(2G_l)$ versus $\gamma = m\pi a/L$ at the onset of bifurcation. The circumferential mode number n varies from 0 to 7. All parameters same as those used in Figure 2 except $b/a = 3$

To investigate the effect of transverse anisotropy, Figure 5 plots the envelope of the bifurcation stress for $G_t/G_l = 0{\cdot}5$, comparing to 0·75 used in Figure 2. All other parameters used in these figures remain the same. By superimposing the results on these two figures, one finds that a hollow cylinder with higher degree of anisotropy is more conducive to diffuse modes of bifurcation. All other features of the bifurcation stress are similar to those discussed for Figure 2.

In most of the experiments for hollow cylinder tests, compressive confining stress is applied on both the inner and outer curved surfaces. Therefore, Figure 6 shows the envelope of the bifurcation stress $s = (\sigma_{zz} - \sigma_{rr})/(2G_l)$ for the case $\sigma_{rr}/G_l = -0{\cdot}02$ and all other parameters are the same as those used in Figure 2. Careful comparison for Figures 2 and 6 shows that the applied compressive stress σ_{rr} reduces the bifurcation stress level under compression ($s < 0$) while increases it under extension ($s > 0$). That is, as expected, hollow cylinders subject to equal internal and external confining stresses are more conducive to bifurcations under compression, but less conducive to bifurcations under extension.

So far, we have been assumed in all the previous numerical calculations that the hollow cylinders made of geomaterials obey the normality flow rule by setting $\beta = \mu = 0{\cdot}4$. Therefore, Figure 7 illustrates the effect of non-normality by setting $\beta \neq \mu$ with $\beta = 0{\cdot}3$ and $\mu = 0{\cdot}5$ in this example. If we superimpose the stress envelope with those given in Figure 2, we find that geomaterials not obeying the normality rule are more conducive to bifurcations than those geomaterials solids obeying the normality rule. Since most geomaterials, such as rock, do not

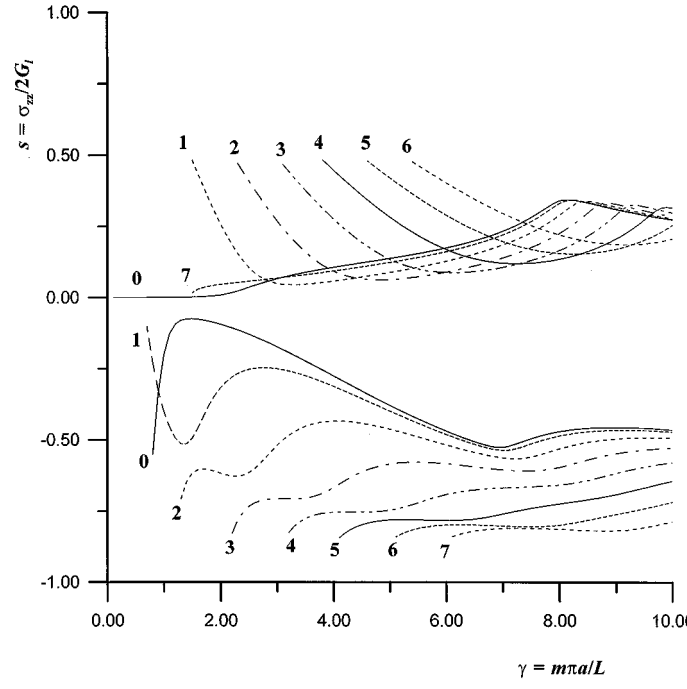

Figure 5. Normalized stress $s = \sigma_{zz}/(2G_l)$ versus $\gamma = m\pi a/L$ at the onset of bifurcation. The circumferential mode number n varies from 0 to 7. All parameters same as those used in Figure 2 except $G_t/G_l = 0{\cdot}5$

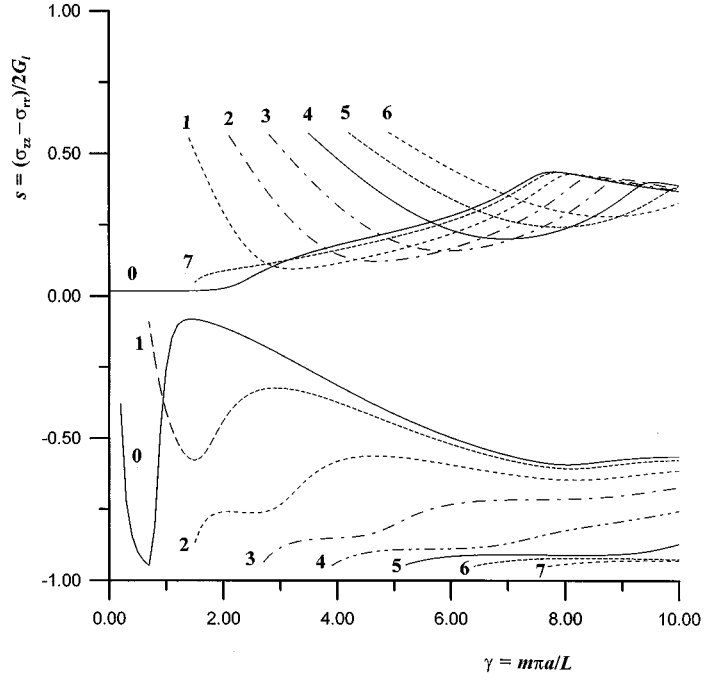

Figure 6. Normalized stress $s = (\sigma_{zz} - \sigma_{rr})/(2G_l)$ versus $\gamma = m\pi a/L$ at the onset of bifurcation. The circumferential mode number n varies from 0 to 7. All parameters same as those used in Figure 2 except $\sigma_{rr}/G_l = -0{\cdot}02$

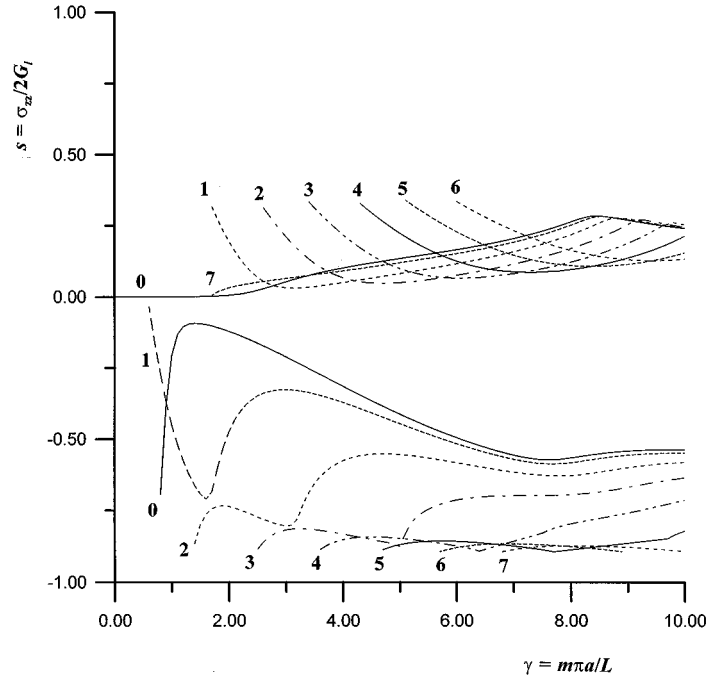

Figure 7. Normalized stress $s = \sigma_{zz}/(2G_l)$ versus $\gamma = m\pi a/L$ at the onset of bifurcation. The circumferential mode number n varies from 0 to 7. All parameters same as those used in Figure 2 except $\mu = 0{\cdot}5$ and $\beta = 0{\cdot}3$

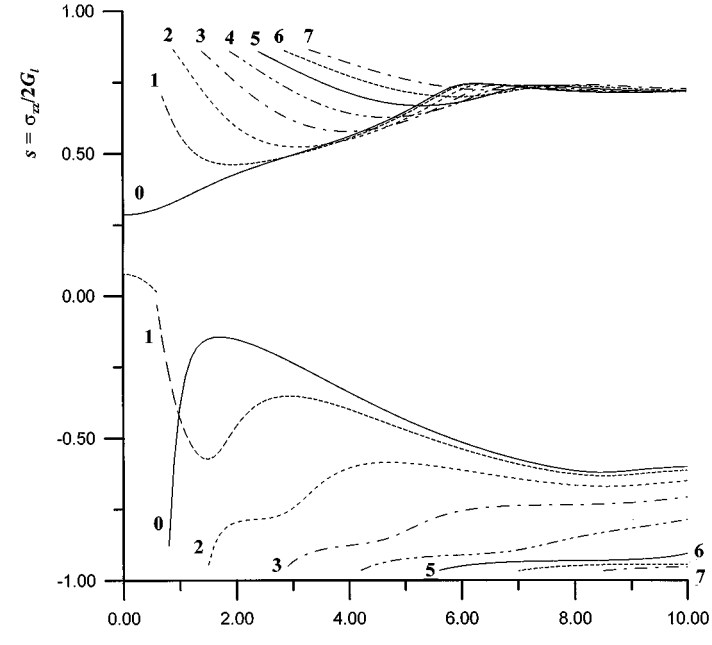

Figure 8. Normalized stress $s = \sigma_{zz}/(2G_l)$ versus $\gamma = m\pi a/L$ at the onset of bifurcation. The circumferential mode number n varies from 0 to 7. All parameters same as those used in Figure 2 except $E/G_l = 0$

obey normality flow rule, and hence are more conducive to diffuse mode bifurcations than other engineering materials, such as metals.

All the previous calculations have been restricted to the cases that bifurcation occurs at the peak applied load or $E = 0$; therefore, Figure 8 presents the results for $E/G_l = 0{\cdot}25$ (and all other parameters remain the same as those used in Figure 2) and clearly illustrates that diffuse mode bifurcation can also occur in the hardening regime of the stress–strain curve or for $E > 0$. However, the stress level required for the onset of bifurcation in the pre-peak regime (by assuming $E > 0$ in (23)) is, in general, larger than those required at the peak applied stress (by assuming $E = 0$ in (23)). The possibility of this kind of pre-peak bifurcation relies on how important is the yield vertex effect on the variation of G_l, as it may drop significantly from its elastic value such that s increases to meet the bifurcation condition given in (23). More discussions on the yield vertex effect can be found in References 5, 36 and 56.

7. CONCLUSIONS

In recent years, thick-walled hollow cylinders have been found extremely useful in the testing of both soils and rocks. For examples, it has been used in estimating shear moduli subject to abrupt changes in the pattern of stress, in simulating borehole instabilities, and in modelling the failure mechanism of breakout near openings such as tunnels.

Therefore, in this paper, we have derived analytically the condition for the onset of diffuse mode bifurcations in thick-walled hollow circular cylinders with internal radius a, external radius b and length L under end compression σ_{zz} and confining stress σ_{rr} on both the inner and outer curved surfaces. In fact, our bifurcation analysis also applies to cylinders subject to extension tests. The geomaterial of our specimen is characterized by the incremental linear model of Rudnicki,[36] and the method of solution for the bifurcation problem uses the velocity potential approach by Chau.[38, 41] As expected, numerical results show that thick-walled cylinders are stronger than thin-walled cylinders against diffuse mode bifurcations, including both buckling, axisymmetric and non-axisymmetric deformations. Under compression, only buckling or anti-symmetric bifurcation (with $n = 1$) and axisymmetric bifurcation (with $n = 0$) are possible, where n is the circumferential mode number assumed in our diffuse mode of deformations given in (17). In contrast to the bifurcation analysis for solid cylinders,[38, 41] no buckling solution is found for γ smaller than 0·7 when b/a is finite and fixed. That is, no buckling for long and slender hollow cylinders with small a/L is found, provided that a/b is fixed and finite. When $0{\cdot}7 < \gamma = m\pi a/L < 0{\cdot}9$, anti-symmetric buckling is the expected bifurcation; whereas, when $\gamma > 0{\cdot}9$, axisymmetric bulging or barrelling is anticipated, where m is the longitudinal mode number defined in (17). The exact value of γ that separates the buckling and barrelling phenomena depends on the values of the constitutive parameters of the geomaterial at the instant of bifurcation. Hollow cylinders with higher degree of anisotropy, disobeying the rule of normality, and subjected to compressive confining stress are found more conducive to bifurcations than cylinders made of materials with isotropy, obeying normality, and subjected to no confining stress.

Numerical results also reveal that pre-peak bifurcation of diffuse modes is always possible and can occur preceding the formation of shear band or strain localization. As a result, the diffuse mode bifurcation considered in this study may result in or act as a trigger for the premature localization of deformation (i.e. localization preceding the prediction by material instability). However, the possible link between these diffuse modes of bifurcation and the localized mode of deformation requires further study.

ACKNOWLEDGEMENTS

The first author's (KTC) interest in hollow cylinder tests was initiated by Prof. A. Drescher when KTC visited University of Minnesota in Spring, 1991. This research was, however, first started when KTC was visiting the Division of Petroleum Resources of CSIRO, Syndal Victoria, Australia in the summer of 1994. KTC is grateful for the financial support by The Hong Kong Polytechnic University and the second author (SKC) of CSIRO for having made the visit possible. Subsequent analysis was done when KTC was under the support of RGC Earmarked Grant Nos. 0357-052 and 0357-025. The authors are grateful to D.E. Amos of Sandia National Laboratories for putting his package up in the internet.

APPENDIX

Boundary conditions in terms of the velocity potentials Φ *and* Ψ

Substitution of (8) and (9) into the relations between velocity field and the nominal stress rate, one obtains the following form of the boundary conditions (3) in terms of the velocity potentials Φ and Ψ:

$$\left(Y_1\nabla_1 + Y_2\frac{\partial^2}{\partial z^2}\right)\frac{\partial\Phi}{\partial z} + Y_3\left[\frac{\partial^3\Phi}{\partial z\,\partial r^2} + \frac{\partial}{\partial r}\left(\frac{1}{r}\frac{\partial\Psi}{\partial\theta}\right)\right] = 0 \tag{38}$$

$$\left(Y_4\frac{\partial}{\partial r}\nabla_1 + Y_5\frac{\partial^3}{\partial r\,\partial z^2}\right)\Phi + Y_6\frac{1}{r}\frac{\partial^2\Psi}{\partial\theta\,\partial z} = 0 \tag{39}$$

$$Y_3\frac{\partial}{\partial r}\left(\frac{1}{r}\frac{\partial^2\Phi}{\partial\theta\,\partial z}\right) + Y_7\left(\frac{1}{r}\frac{\partial\Psi}{\partial r} + \frac{1}{r^2}\frac{\partial^2\Psi}{\partial\theta^2}\right) - Y_8\frac{\partial^2\Psi}{\partial r^2} = 0 \tag{40}$$

on $r = a, b$, where

$$Y_1 = \frac{9K}{4} - G_t + \sigma_{rr} - \frac{(9K/4 + G_t)(9K\nu/2 + \sigma_{rr})}{9K\nu/2 + G_l(1-s)}, \qquad Y_2 = -\frac{G_l(1+s)(9K\nu/2 + \sigma_{rr})}{9K\nu/2 + G_l(1-s)} \tag{41}$$

$$Y_3 = 2G_t - \sigma_{rr}, \qquad Y_4 = -\frac{G_l(1-s)(9K/4 + G_t)}{9K\nu/2 + G_l(1-s)}, \qquad Y_5 = \frac{G_l(1-s)(9K\nu/2 - 2G_ls)}{9K\nu/2 + G_l(1-s)} - \sigma_{rr} \tag{42}$$

$$Y_6 = G_l(1-s) - \sigma_{rr}, \qquad Y_7 = G_t - \sigma_{rr}, \qquad Y_8 = G_t \tag{43}$$

REFERENCES

1. F. D. Adams, 'An experimental contribution to the question of the depth of the zone of flow in the Earth's crust', *J. Geol.*, **20,** 97–118 (1912).
2. W. M. Kirkpatrick, 'The condition of failure of sands', *Proc. 4th Int. Conf. Soil Mech. Found. Engng.*, Vol. 1, 1957, pp. 172–178.
3. T. E. Tullis and J. Tullis, 'Experimental rock deformation techniques', in B. E. Hobbs and H. C. Heard (eds.), *Mineral and Rock Deformation: Laboratory Studies* (*The Paterson Volume*), Geophysical Monograph 36, AGU, Washington D.C., 1988, pp. 297–324.
4. W. R. Wawersik, J. W. Rudnicki, W. A. Olsson, D. J. Holcomb and K. T. Chau, 'Localization of deformation in brittle rock: theoretical and laboratory investigation', in S. P. Shah, S. E. Swartz and M. L. Wang (eds.), *Micromechanics of Failure of Quasi-brittle Materials*, Albuquerque, NM, 6–8, June, Elsevier Applied Science, 1990, pp. 115–124.

5. J. W. Rudnicki and J. R. Rice, 'Conditions for the localization of deformation in pressure-sensitive dilatant materials', *J. Mech. Phys. Solids* **23,** 371–394 (1975).
6. K. T. Chau and J. W. Rudnicki, 'Bifurcations of compressible pressure-sensitive materials in plane strain tension and compression', *J. Mech. Phys. Solids*, **38,** 875–898 (1990).
7. P. W. Bridgman, 'The failure of cavities in crystals and rocks under pressure', *Am. J. Sci*., **45,** 243–269 (1918).
8. E. C. Robertson, 'Experimental study of the strength of rocks', *Bull. Geol. Soc. Am.* **66,** 1275–1314 (1955).
9. E. R. Hoskins, 'Failure of thick walled hollow cylinders of isotropic rocks', *Int. J. Rock Mech. Min. Sci*., **6,** 99–125 (1969).
10. J. J. K. Daemen and C. Fairhurst, 'Influence of failed rock properties on tunnel stability', in *Dynamics Rock Mechanics*, *Proc. 12th U.S. Symp. on Rock Mechanics*, Rolla, 1970, pp. 855–875.
11. M. B. Dusseault, 'A versatile hollow cylinder triaxial device', *Can. Geotech. J*., **18,** 1–7 (1981).
12. F. J. Santarelli, E. T. Brown and V. Maury, 'Analysis of borehole stresses using pressure dependent, linear elasticity', *Int. J. Rock Mech. Min. Sci Geomech. Abstr*., **23,** 445–449 (1987).
13. R. T. Ewy and N. G. W. Cook, 'Deformation and fracture around cylindrical openings in rock—I: observation and analysis of deformations', *Int. J. Rock. Mech. Min. Sci. Geomech. Abstr*., **27,** 387–407 (1990).
14. M. A. Addis and B. Wu, 'The role of the intermediate principal stress in welbore stability studies: evidence from hollow cylinder tests', *Int. J. Rock Mech. Min. Sci. Geomech. Abstr*., **30,** 1027–1030 (1993).
15. A. Guenot, 'Contraintes et ruptures autour de forages petroliers', *Proc. 6th Congr. ISRM*, *Montreal*, Vol. 1, Balkema, Rotterdam, 1987, pp. 109–110.
16. P. J. Perie, *Experimental investigation of welbore stability*, *Ph.D. Thesis*, University of California, Berkeley, 1989.
17. P. J. Perie and R. E. Goodman, 'Evidence of new failure patterns in a thick-walled cylinder experiment', *Proc. 12th Annual Energy Sources Technol. Conf. and Exhibition*, *Drilling Symp*., ASME, New York, 1989, pp. 23–27.
18. F. J. Santarelli and E. T. Brown, 'Failure of three sedimentary rocks in triaxial and hollow cylinder compression tests', *Int. J. Rock Mech. Min. Sci. & Geomech. Abstr*. **26,** 401–413 (1989).
19. N. C. Gay, 'Fracture growth around openings in thick-walled cylinders of rock subjected to hydrostatic compression', *Int. J. Rock Mech. Min. Sci. Geomech. Abstr*. **10,** 209–233 (1973).
20. S. K. Choi, The bearing capacity of foundations in weak rock, *Ph.D. Thesis*, Monash University, Australia, 1984.
21. I. W. Johnston and S. K. Choi, 'A synthetic soft rock for laboratory model studies', *Geotechnique* **36,** 251–236 (1986).
22. R. Cox, private communication, 1994.
23. T. H. Wu, A. K. Loh and L. E. Malvern, 'Study of failure envelope of soils', *J. Soil Mech. Found. Eng. Div. ASCE* **89**(SMI), 145–181 (1963).
24. M. Fahey, 'Expansion of a thick cylinder of sand: a laboratory simulation of the pressuremeter test', *Geotechnique*, **36,** 397–424 (1986).
25. A. Alsiny, Deformation modes in a thick-walled hollow cylinder experiment on dry sand, *Ph.D. Thesis*, University of Minnesota, U.S.A., 1992.
26. A. Alsiny, I. G. Vardoulakis and A. Drescher, 'Deformation localization in cavity inflation experiments on dry sand', *Geotechnique*, **42,** 365–410 (1992).
27. B. Kambe, 'Experimental recrystallization of ice under stress', in H. C. Heard, I. Y. Borg, N. L. Carter, and C. B. Raleigh (eds.), *Flow and Fracture of Rocks: The Griggs Volume,* Geophysical monograph 16, AGU, Washington D.C., 1972, pp. 211–241.
28. M. A. Biot, Hodograph method of nonlinear thick-walled cylinders and spheres, including porous materials, *Int. J. Solids Struct*. **12,** 613–618 (1976).
29. A. Pellegrino, J. Sulem and G. Barla, 'Non-linear effects in the study of borehole stability', *Eurock'94*, Balkema, Rotterdam, 1994, pp. 231–238.
30. I. G. Vardoulakis, J. Sulem and A. Guenot, 'Borehole instabilities as bifurcation phenomena', *Int. J. Rock Mech. Min. Sci. Geomech. Abstr*., **25,** 159–170 (1988).
31. I. G. Vardoulakis and P. C. Papanastasiou, 'Bifurcation analysis of deep boreholes: I. Surface instabilities', *Int. J. Numer. Anal. Meth. Geomech*., **12,** 379–399 (1988).
32. P. C. Papanastasiou and I. G. Vardoulakis, 'Bifurcation analysis of deep boreholes: II. Scale effect', *Int. J. Numer. Anal. Meth. Geomech*., **13,** 183–198 (1989).
33. P. C. Papanastasiou and I. G. Vardoulakis, 'Numerical treatment of progressive localization in relation to borehole stability', *Int. J. Numer. Anal. Meth. Geomech*., **16,** 389–424 (1992).
34. G. A. Kardomateas, 'Buckling of thick orthotropic cylindrical shells under external pressure', *J. Appl. Mech. ASME*, **60,** 195–202 (1993).
35. G. A. Kardomateas, 'Stability loss in thick transversely isotropic cylindrical shells under axial compression', *J. Appl. Mech. ASME* **60,** 506–513 (1993).
36. J. W. Rudnicki, 'The effect of stress-induced anisotropy on a model of brittle rock failure as localization of deformation', in *Energy Resources and Excavation Technology*, *Proc. 18th U.S. Symposium on Rock Mechanics*, Keystone, Colorando, 22–24, June, 1977, pp. 3B4-1–3B4-8.

37. K. T. Chau, 'Non-normality and bifurcation in a compressible pressure-sensitive circular cylinder under axisymmetric tension and compression', *Int. J. Solids Struct.* **29,** 801–824 (1992).
38. K. T. Chau, 'Antisymmetric bifurcations in a compressible pressure-sensitive circular cylinder under axisymmetric tension and compression', *J. Appl. Mech. ASME*, **60,** 282–289 (1993).
39. K. T. Chau, 'Bifurcations at a spherical cavity in a compressible solid with spherical isotropy', *Int. J. Numer. Anal. Meth. Geomech.*, **19,** 381–398 (1995).
40. H.-C. Hu, 'On the three-dimensional problems of the theory of elasticity of a transversely isotropic body', *Acta Scientia Sinica*, **2,** 145–151 (1954).
41. K. T. Chau, 'Buckling, barrelling, and surface instabilities of a finite, transversely isotropic circular cylinder', *Quart. Appl. Math.* **53,** 225–244 (1995).
42. P. J. van den Hoek, A. P. Kooijman, C. J. Kenter, M. Khodaverdian, C. R. Hyland and J. D. McLennan, 'Size-dependency of hollow cylinder collapse strength', *67th Annual Technical Conf. and Exhibition of the SPE*, Washington, DC, SPE 24800, II, 1992, pp. 351–360.
43. Z. P. Bazant, F.-B. Lin and H. Lippmann, 'Fracture energy release and size effect in borehole breakout', *Int. J. Numer. Anal. Meth. Geomech.*, **17,** 1–14 (1993).
44. A. V. Dyskin and L. M. Germanovich, 'Model of rock burst caused by cracks growing near free surface', in: P. Young (ed.), *Rockburst and Seismicity in Mines 93*, Balkema, Rotterdam, 1993, pp. 169–175.
45. L. N. Germanovich, J. C. Roegiers and A. V. Dyskin, 'A model for borehole breakouts in brittle rocks', *Eurock'94*, Balkema, Rotterdam, 1994, pp. 361–370.
46. W. Prager, *Introduction to the Mechanics of Continua*, Dover, New York, 1973.
47. W. H. Press, B. P. Flannery, S. A. Teukolsky and W. T. Vetterling, *Numerical Recipes: The Art of Scientific Computing,* 2nd edn, Cambridge University Press, New York, 1992.
48. S. Chang and J.-M. Jin, *Computation of Special Functions*, Wiley, New York, 1996.
49. D. E. Amos, *Computation of Bessel function of complex argument and large order*, SAND83-0643, Sandia National Laboratory, Albuquerque, U.S.A., 1983.
50. D. E. Amos, *A subroutine package for Bessel functions of a complex argument and non-negative order*, SAND85-1018, Sandia National Laboratory, Albuquerque, U.S.A., 1985.
51. D. E. Amos, 'A portable package for Bessel functions of a complex argument and nonnegative order', *ACM Trans. Math. Software*, **12,** 265–273 (1986).
52. D. E. Amos, 'Remark on algorithm 644', *ACM Trans. Math. Software*, **16,** 404 (1990).
53. D. E. Amos, 'A remark on algorithm 644: A portable package for Bessel functions of a complex argument and nonnegative order', *ACM Trans. Math.. Software*, **21,** 388–393 (1995).
54. H. Bateman, *Table of the Bessel functions $J_0(z)$ and $J_1(z)$ for Complex Arguments*, Columbia University Press, New York, 1947.
55. M. Abramowitz and I. A. Stegun, *Handbook of Mathematical Functions*, Dover, New York, 1965.
56. J. W. Rudnicki, 'A class of elastic-plastic constitutive laws for brittle rocks', *J. Rheology*, **28,** 759–778 (1984).

